

Modelling compressive crush of composite tube reinforced foam sandwiches

* Jin Zhou¹, Zhongwei Guan¹ and Wesley Cantwell²

¹School of Engineering, University of Liverpool, Liverpool L69 3GQ, UK

²Aerospace Research and Innovation Center (ARIC), Khalifa University of Science , Technology and Research, Abu Dhabi, UAE

*Jin Zhou: jinzhou@LIV.AC.UK

Abstract

The finite element (FE) models were developed to predict the compressive response and energy-absorbing capability of composite tube reinforced PVC foams. A vectorized user material subroutine (VUMAT) was employed to define Hashin's 3D damage criteria for the composite tube to model the corresponding deformation and failure mechanisms. Good agreement was obtained in terms of the load–displacement traces, the deformation and failure modes. Using validated models, parametric studies were further carried out to investigate the crushing characteristics of composite tube reinforced foam to optimize the composite tube configurations within the foam.

It has been shown that reinforcing the foams with composite tubes results in a significant increase in both their compressive strength and energy absorption relative to their plain counterparts. It has also been shown that the 12.5 mm carbon fibre tube reinforced foam out-performs the 10 and 8 mm tube reinforced foam based sandwich panel in term of energy absorption. The energy absorption increased with increasing of both foam density and tube diameters.

Keywords: Finite Element, Hashin 3-D Criteria, User-defined subroutine, Carbon tube reinforced foam, Energy absorption.

Introduction

As a result of their superior specific strength and stiffness characteristics, excellent fatigue properties and impressive corrosion resistance, composite materials, such as carbon fibre reinforced plastic (CFRP) are currently finding widespread use in a wide range of high-performance engineering structures. An additional attractive feature of these lightweight materials is their ability to absorb significant energy under certain well-defined loading conditions. Extensive testing has shown that composites, when produced in a tubular form and loaded in compression, are capable of absorbing significant energy through a range of failure mechanisms including fibre fracture, matrix cracking, debonding and delamination [Farley and Jones (1992)]. Over the years, this impressive energy-absorbing capability has attracted the interest of many vehicle manufacturers, including Chrysler and Ford. Indeed, [Jacob et al. (2002)] calculated that only 600 grams of composite is required to absorb the energy of a medium-sized car travelling at 35 mph. Alia investigated the energy-absorbing characteristics of polymer foams reinforced with small carbon fibre reinforced epoxy tubes [Alia et.al 2014]. Figure 1a highlights the extraordinary failure characteristics associated with composite materials, where a 10 mm diameter CFRP tube is being crushed at a low rate of strain. These images give evidences that these failure modes of carbon tube are typical ones of those observed in larger diameter tubes, with extensive splaying, fibre fracture and matrix cracking. Zhou et al. investigated the failure mechanism and energy absorption capacity of both carbon and glass rods experimentally. The progress failure of carbon and glass fibre rods subjected to compression was examined and shown in Figure 1b that the carbon fibre rod under compression demonstrates more ductile failure than the glass fibre one [Zhou et al. (2013)]. Clearly, the failure

pattern of the rod influences its energy absorbing capacity. If buckling failure can be avoided the energy absorption will be maximized. Therefore, it is necessary to introduce constraints to composite tubes or rods. An effective way to apply such constraints is to embed them into PVC foam, so that a progressive crushing of composite tube or rod can be realised. The study exhibits failed PVC foam core with embedded carbon fibre and glass fibre pins. Both carbon and glass fibre rods turn into dust, which indicate tests with successful constraints offered by PVC foam. The energy-absorbing capacity of a composite tube or rod is most frequently evaluated by determining its specific energy absorption (SEA) capability in J/kg. SEA values can vary greatly, for example, from 20 kJ/kg for a pultruded glass fibre/epoxy [Jacob et al. (2002)] to values well in excess of 100 kJ/kg for carbon fibre-based systems [Hamada (1993)]. The precise value depends on a number of parameters, including the geometry of the tube, its fibre architecture, as well as the mechanical properties of the matrix phase. For example, Hamada and co-workers showed that the energy-absorbing capacity of a 55 mm diameter CFRP tube decreased by fifteen percent in passing from a unidirectional tube to one with its fibres oriented at $\pm 25^\circ$. A number of researchers have studied the influence of specimen geometry on the energy-absorbing capability of composite tubes. [Thornton et al. (1979); Thornton and Edwards (1982)] investigated geometrical effects in the energy-absorbing response of tubes based on circular, square and rectangular cross-sections and showed that the former out-performed both their square and rectangular tubular counterparts. [Farley et al. (1986)] conducted tests on carbon and Kevlar fibre reinforced tubes, with ply orientations typical of those used in sub-floor beam structures and showed that the tube diameter to thickness ratio played a significant role in determining its subsequent strain energy-absorbing capacity. Similar trends have been observed by [Alia et al. (2014)] following tests on circular composite tubes, with values increasing by over fifty percent as the D/t ratio is reduced from approximately 42 to 6. This evidence suggests that the use of very low values of D/t can lead to greatly enhanced energy absorption in tubular structures. Following these initial tests on small diameter reinforcements, individual tubes were embedded in a polymer foam and crushed at quasi-static rates of strain



Figure 1 Failure modes of the composite tube and rods subject to crushing load (a. tube, b. rods)

Composite sandwich structures are increasingly finding use in a wide range of lightweight load-bearing engineering structures. Sandwich structures, such as those used in high-performance aerospace components, are typically based on thin composite. The variation of the specific energy absorption of circular CFRP tubes with diameter/thickness ratio by [Alia et al. (2014)]. The tube embedded in a polymer foam and skins bonded to a low density foam or honeycomb core. The skins are usually thin, often rendering these lightweight panels highly susceptible to damage by a hard projectile, such as that associated with runway debris or hail. A number of investigations have focused on the potential hazard resulting from an uncontained turbine engine failure on outer parts of an aircraft [Shockey (1997), Rouse et.al (1997)]. In such sandwich structures, the skin sheets carry bending loads, whilst the core resists transverse shear and through-thickness indentation forces. Therefore, to enhance the load carrying capacity it is desirable to maximize the through-thickness stiffness and strength of the core. One approach to achieve this goal is to add reinforcing pins to the core, with the ends of the pins embedded in woven carbon fibre skin sheets. [Cartie and Fleck (2003)] undertook the theoretical analysis and revealed that the through-thickness stiffness

and strength are relatively insensitive to the pin arrangements in pyramidal, tetrahedral and random patterns.

Since experimental trials are usually time-consuming and costly, it is evident that modelling the crushing behavior to investigate the energy-absorbing characteristics using commercial finite element software would be of great interest. Once these models are verified, they can be used to predict the response of rods and tube reinforced foam based on different configurations, loading and boundary conditions without undertaking experimental tests. A number of numerical works have been carried out to modeling the response of composite tubes. Carla McGregora developed a model to predict the damage propagation, failure mode and energy absorption in triaxially braided composite tubes under axial compression using LS-DYNA [Carla McGregora et al. (2010)]. The two-ply and four-ply square tubes were modeled to predict energy absorbing of front rail structures components on vehicular under axial crushing. A micromechanical model incorporated as a subroutine coded into the ABAQUS implicit by [Beard and Chang (2002)] to simulate the complete crushing process of plug-initiated triaxially braided composite tubes with promising initial results. The developed model was incorporated into ABAQUS/Explicit to model dynamic response of tube under crushing load by [Flesher (2006)]. Another damage model on composite (Mat_58) in LS-DYNA with a lower accuracy than the predicted SEA values of un-initiated tubes were 30-40% lower than experimental results [Xiao et al. (2009)]. A developed model for composite tube was only able to capture the axial crushing features of plug-initiated braided composite tubes accurately [C.J. McGregor et al. (2007)], however the simulation of this model on un-initiated tubes was not successful on failure modes due to model instability, there were discrepancies between predicted and observed failure modes.

It is a challenging task to develop a model that is able to capture both the energy absorption and failure mode. A few researchers have attempted to model crushing of composite tubes and to simulate a similar splaying mode of failure. Mamalis et al. developed a finite element modeling to simulate axial collapse of CFRP square tubes under static and dynamic load. The model introduced a third layer to model the resin layer into pulverized debris during axial crushing. The deletion of the failure elements in the middle layer resulted in a low energy absorption [Mamalis et al. (2006)]. A splaying mode of failure on glass/polyester tubes has been developed by Silcock et al. using LS-DYNA [Silcock et al. (2006)]. The model employed a spotweld approach and pre-defining a debris wedge to simulate a delamination, initiation and propagation of the splaying failure mode. Although the failure modes were simulated successfully, the correlation between measured and predicted load-displacement profiles was lower. The most successful model to simulate the splaying mode of failure on tube was developed by Pinho et al. using a decohesion element incorporated into ABAQUS. Both the delamination and the transverse tearing through thickness between the composite layers were simulated. Both the load and failure modes were captured reasonably, however only a portion of the propagation during the crushing process was modeled. [Pinho et al. (2004)]

Although a few numerical models were developed to simulate the response of composite using commercial software LS-DYNA and Abaqus. However, those such as ABAQUS only has a number of failure criteria for composite materials modeled using 2D elements, such as plane stress and continuum shell elements [Carla McGregora (2010)]. Further, none of these criteria consider strain-rate effects in composite materials, which is clearly important in dynamic studies. The 2D elements, with the existing failure criteria, are not capable of taking large through-the-thickness rate-dependent deformations into account. Therefore, it is necessary to develop a constitutive model with associated failure criteria suitable for simulating a composite material using 3D solid elements. Limited numerical modeling was developed to investigate the structural response of composite using three-dimensional 3D solid elements. Recently, Thuc et al. developed a FE model which were

validated using experimental data from tests on FMLs based on a 2024-O aluminium alloy and a woven glass–fibre/polypropylene composite. The rate-dependent failure criteria for a unidirectional composite were used, which were based on the modified Hashin’s 3D failure criteria [Thuc et al. (2013)]. The constitutive model and failure criteria were then implemented in ABAQUS/Explicit using the VUMAT subroutine. Based on the previous research [Thuc et al. (2013)], A further parametric studies were carried out to investigate the influence of the properties of the aluminium alloy on the blast resistance of FMLs for aerospace applications. A vectorized user material subroutine (VUMAT) was employed to define Hashin’s 3D rate-dependant damage constitutive model of the GFPP. [Thuc et al. (2014)] Sandwich panels based on three-dimensional woven S-glass/epoxy skins and a crosslinked PVC core were modelled using finite element techniques to investigate the effect of through-the-thickness stitching on the blast resistance of the panels by [Guan et al. (2014)]. The finite element model accurately predicted the failure modes and deformed shapes of the sandwich panels over the range of impulsive loading conditions.

The superior mechanical properties provided by a roll wrapped composite tube manufactured predominantly using high modulus (T700) unidirectional pre-preg carbon fibre oriented to provide maximum strength in the lateral (length-ways) axis, also the use of pre-preg reinforcement oriented at 90° to ensures that the tube has good crush/burst strength around the section of the tube. Their superior mechanical properties offers special energy absorption which mean that tubes of the same weight as an aluminium or steel tube can be much stronger, or that tubes of the same strength can be much lighter, contribute more energy absorption subject to compressive crushing.

This paper presents numerical modeling of compressive structural behavior of PVC foam core panels reinforced by CFRP tubes. Here, the foam was modeled as a crushable foam material with strain hardening. A vectorized user material subroutine (VUMAT) was employed to define Hashin’s 3D damage criteria for the composite tube to model the corresponding deformation and failure mechanisms. Energy absorption of the sandwich panels made with different densities of the cores was also investigated. Modeling results were compared with the experimental results, in terms of load-displacement relationships, deformation and failure modes. Reasonably correlation was obtained.

2 Finite element modeling

2.1 PVC foam

Numerical models were developed to simulate the mechanical response of the tube reinforced foam subjected to comparison. The PVC foam core in the structure was modeled as a crushable foam subjected to compressive loading with rate-dependent strain hardening and both shear and ductile failure criteria. It was assumed that the Poisson’s ratio of all of the foams was 0.32. The phenomenological yield surface proposed by [Deshpande and Fleck (2001)] for a closed-cell foam material, given by:

$$\phi \equiv \left[\frac{1}{1 + (\alpha/3)^2} \right] [q^2 + \alpha^2 \sigma_m^2] - \sigma_y^2 \leq 0 \quad (1)$$

where σ_y is the uniaxial yield strength of the foam in tension or compression, q is the Von Mises stress, and σ_m is the mean stress. The term α defines the shape of the yield surface, which is given by

$$\alpha = \frac{3k}{\sqrt{(3k_t + k)(3 - k)}} \quad (2)$$

where k and k_t are related to the ratios of the initial uniaxial yield stress σ_c^o and the hydrostatic tensile yield stress p_t to the hydrostatic compressive yield stress p_c^o , respectively.

The yield stress in hydrostatic compression, p_c describes the development of the size of the yield surface and is given as:

$$p_c(\varepsilon_{pl}^{vol}) = \frac{\sigma_c(\varepsilon_{pl}^{vol}) \left[\sigma_c(\varepsilon_{pl}^{vol}) \left(\frac{1}{\alpha^2} + \frac{1}{9} \right) + \frac{p_t}{3} \right]}{p_t + \frac{\sigma_c(\varepsilon_{pl}^{vol})}{3}} \quad (3)$$

where ε_{pl}^{vol} is defined as the plastic volumetric strain in the volumetric hardening model, and is set equal to ε_{pl}^{axial} the compressive plastic strain. The term, p_c can therefore be determined from a compression test on the foam. Mechanical properties of the foams investigated are shown in Table 1.

Here, it is assumed that the response of a rate-dependent solid obeys the uniaxial flow rate definition, which is given as:

$$\dot{\bar{\varepsilon}}_{pl} = h(q, \bar{\varepsilon}_{pl}, \theta) \quad (4)$$

in which the term h is a strain-hardening function, $\bar{\varepsilon}_{pl}$ is defined as the equivalent plastic strain, and the parameter θ is the temperature. The rate-dependent hardening curves can therefore be expressed as:

$$\bar{\varepsilon}(\bar{\varepsilon}_{pl}, \dot{\bar{\varepsilon}}_{pl}) = \sigma_y(\bar{\varepsilon}_{pl}) R(\dot{\bar{\varepsilon}}_{pl}) \quad (5)$$

in which $\dot{\bar{\varepsilon}}_{pl}$ and R are defined as the equivalent plastic strain-rate and the stress ratio ($= \bar{\sigma} / \sigma_y$) respectively, which are given as:

$$\bar{\varepsilon}_{pl} = \int_0^t \sqrt{\frac{2}{3} \dot{\bar{\varepsilon}}_{pl} : \dot{\bar{\varepsilon}}_{pl}} dt \quad \text{and} \quad R = \bar{\sigma} / \sigma_y \quad (6)$$

Damage initiation in the PVC foam was modelled by applying a ductile damage criterion combined with a shear damage criterion. The former assumes that the equivalent plastic strain at the onset of damage is a function of the stress triaxiality (ratio of the pressure stress to the effective stress) and strain-rate. The latter criterion assumes that the equivalent plastic strain at the onset of damage is a function of the shear stress ratio and strain-rate. The fracture strains corresponding to the initiation of ductile damage and shear damage and the related strain-rate need to be specified.

Table 1 Mechanical properties of the foams investigated used in this study [Zhou et al. (2012)].

	C40	C80	C130	C200
Density (kg/m ³)	40	80	130	200
Compressive modulus (MPa)	37	97	160	280
Compressive strength (MPa)	0.45	1.3	2.6	4.8
Compressive fracture strain	0.65	0.7	0.7	0.7
Tensile modulus (MPa)	28	66	110	175
Tensile strength (MPa)	0.7	2.0	3.8	6.0
Shear modulus (MPa)	13	30	47	75
Shear strength (MPa)	0.5	1.2	2.3	3.5
Shear fracture strain	0.08	0.23	0.30	0.30
Work of fracture in tension (kJ/m ²)	0.21	0.44	0.76	1.33
Work of fracture in shear (kJ/m ²)	4.5	12.6	27.6	44.2

2.2 CFRP Tube

2.2.1 Carbon fibre woven composites

The superior mechanical properties provided by a composite tube manufactured predominantly using high modulus (T700) unidirectional pre-preg carbon fibre oriented to provide maximum strength in the lateral (length-ways) axis, also the use of pre-preg reinforcement oriented at 90° to ensures that the tube has good crush/burst strength around the section of the tube. Given that a roll wrapped carbon fibre composite tubes are manufactured from special high-modulus Toray T700 unidirectional pre-preg carbon fibre oriented at 0° (down the length of the tube) and unidirectional E-Glass oriented at 90° (around the section of the tube) by placing fibres in a [0,90,0,90,0] pattern. The overall strength of tube equal 50% CF at 0° and 50% CF at 90° direction. A constitutive model and failure criteria suitable for simulating the solid geometry composite using 3D solid elements was employed to summate the failure mechanism of carbon fire tubes.

Failure criteria for laminated composites are available in ABAQUS, which can be applied for panel coordinate and continuum shell elements only. However, none of these existing criteria consider the third direction through-the-thickness and strain-rate effects in the composite material in a cylindrical coordinate system using 3D solid elements. In order to develop a constitutive model and failure criteria suitable for simulating the composite tube using 3D solid elements, a 3D rate-dependent failure criteria for a anisotropic composite is developed by modifying Hashin's 3D failure criteria [Hashin (1980), Thuc et.al (2012)], to include rate-dependent elastic moduli and strength properties. The failure criteria, with the related constitutive model, are implemented into ABAQUS/Explicit using a VUMAT subroutine provided by ABAQUS [ABAQUS Theory Manual. 6.11(2011)].

The material behaviour within the cross section is same in the lateral axis and roll directions according to the material test data provided by the manufacturer. Therefore, the developed Hashin's 3D failure criteria [Thuc et.al (2013)] are able to simulate overall response of a roll wrapped composite layer in a cylindrical coordinate. The failure functions may be expressed as follows:

$$\text{Fibre tension: } (\sigma_{11} \geq 0): F_f^t = \left(\frac{\sigma_{11}}{X_{1t}} \right)^2 + \left(\frac{\sigma_{12}}{S_{12}} \right)^2 + \left(\frac{\sigma_{13}}{S_{13}} \right)^2, d_{ft} = 1 \quad (7)$$

$$\text{Fibre compression: } (\sigma_{11} < 0): F_f^c = \frac{|\sigma_{11}|}{X_{1t}}, d_{fc} = 1 \quad (8)$$

$$\text{Matrix tension: } (\sigma_{22} + \sigma_{33} \geq 0): F_m^t = \frac{(\sigma_{22} + \sigma_{33})^2}{X_{2t}^2} + \frac{\sigma_{23}^2 - \sigma_{22}\sigma_{33}}{X_{23}^2} + \frac{\sigma_{12}^2 + \sigma_{13}^2}{X_{12}^2}, d_{mt} = 1 \quad (9)$$

$$\text{Matrix compression: } (\sigma_{22} + \sigma_{33} \leq 0):$$

$$F_m^c = \left[\left(\frac{X_{2c}}{2S_{23}} \right)^2 - 1 \right] \frac{(\sigma_{22} + \sigma_{33})}{X_{2c}^2} + \frac{(\sigma_{22} + \sigma_{33})^2}{4S_{23}^2} + \frac{\sigma_{23}^2 - \sigma_{22}\sigma_{33}}{X_{23}^2} + \frac{\sigma_{12}^2 + \sigma_{13}^2}{X_{12}^2}, d_{mc} = 1 \quad (10)$$

where X_{1t} , X_{1c} , X_{2t} , X_{2c} , S_{12} , S_{13} and S_{23} are the various strength components [18] and d_{ft} , d_{fc} , d_{mt} and d_{mc} are the damage variables associated with the four failure modes.

The response of the material after damage initiation (which describes the rate of degradation of the material stiffness once the initiation criterion is satisfied) is defined by the following equation:

$$\sigma = C(d) \cdot \varepsilon, \quad \sigma_{ij} = C_{ij} \cdot \varepsilon_{ij} \quad (11)$$

$$\begin{bmatrix} \sigma_{11} \\ \sigma_{22} \\ \sigma_{33} \\ \sigma_{12} \\ \sigma_{23} \\ \sigma_{13} \end{bmatrix} = \begin{bmatrix} C_{11}^0 & C_{12}^0 & C_{13}^0 & & & \\ C_{12}^0 & C_{22}^0 & C_{23}^0 & & & \\ C_{13}^0 & C_{23}^0 & C_{33}^0 & & & \\ & & & C_{44}^0 & & \\ & & & & C_{55}^0 & \\ & & & & & C_{66}^0 \end{bmatrix} \begin{bmatrix} \varepsilon_{11} \\ \varepsilon_{22} \\ \varepsilon_{33} \\ \varepsilon_{12} \\ \varepsilon_{23} \\ \varepsilon_{13} \end{bmatrix} \quad (12)$$

where C_{ij} is a 6 x6 symmetric damaged matrix, whose non-zero terms can be written as:

$$\begin{aligned} C_{11} &= (1 - d_f) E_1 (1 - \nu_{23} \nu_{32}) \Gamma \\ C_{22} &= (1 - d_f) (1 - d_m) E_2 (1 - \nu_{13} \nu_{31}) \Gamma \\ C_{33} &= (1 - d_f) (1 - d_m) E_3 (1 - \nu_{12} \nu_{21}) \Gamma \\ C_{12} &= (1 - d_f) (1 - d_m) E_1 (\nu_{21} - \nu_{31} \nu_{23}) \Gamma \\ C_{23} &= (1 - d_f) (1 - d_m) E_2 (\nu_{32} - \nu_{12} \nu_{31}) \Gamma \\ C_{31} &= (1 - d_f) (1 - d_m) E_1 (\nu_{31} - \nu_{21} \nu_{32}) \Gamma \\ C_{44} &= (1 - d_f) (1 - s_{mt} d_{mt}) E_1 (1 - s_{mc} d_{mc}) G_{12} \\ C_{55} &= (1 - d_f) (1 - s_{mt} d_{mt}) E_1 (1 - s_{mc} d_{mc}) G_{23} \\ C_{66} &= (1 - d_f) (1 - s_{mt} d_{mt}) E_1 (1 - s_{mc} d_{mc}) G_{13} \end{aligned} \quad (13)$$

where the global fibre and matrix damage variables as well as the constant Γ are also defined as:

$$\begin{aligned} d_f &= 1 - (1 - d_{ft}) (1 - d_{fc}) \\ d_m &= 1 - (1 - d_{mt}) (1 - d_{mc}) \\ \Gamma &= 1 / (1 - \nu_{12} \nu_{21} - \nu_{23} \nu_{32} - \nu_{13} \nu_{31} - 2 \nu_{21} \nu_{32} \nu_{13}) \end{aligned} \quad (14)$$

where E_i is the Young's modulus in the i direction, G_{ij} is the shear modulus in the i - j plane and ν_{ij} is the Poisson's ratio for transverse strain in the j -direction, when the stress is applied in the i -direction. The Young's moduli, shear's moduli, Poisson's ratios and strengths of the CFRP are given in Table 2 and 3. The factors s_{mt} and s_{mc} in the definitions of the shear moduli are introduced to control the reduction in shear stiffness caused by tensile and compressive failure in the matrix respectively. The following values are recommended in [ABAQUS Theory Manual (2011)]: $s_{mt} = 0.9$ and $s_{mc} = 0.5$.

Table 2. Properties data for the CFRP tube

E_1 (MPa)	E_2 (MPa)	E_3 (MPa)	G_{12} (MPa)	G_{13} (MPa)	G_{23} (MPa)	ν_{12} (MPa)	ν_{13} (MPa)	ν_{23} (MPa)	ρ (kg/m ³)
70	70	10	8.6	8.6	8.6	0.1	0.3	0.3	1600

Table 3. Damage initiation data for the CFRP tube

X_{1T} (MPa)	X_{1C} (MPa)	X_{2T} (MPa)	X_{2C} (MPa)	S_{12} (MPa)	S_{13} (MPa)	S_{23} (MPa)
600	570	600	570	280	280	280

2.2.2. Strain-rate effects in the mechanical properties

The effects of strain-rate on the mechanical properties of a composite material are typically modelled using strain-rate dependent functions for both the elastic modulus and the strength. Yen developed logarithmic functions to account for strain-rate effects in a composite material as follows [Yen (2012)]:

$$\begin{aligned} \{S_{RT}\} &= \{S_0\} \left(1 + C_1 \ln \frac{\dot{\bar{\epsilon}}}{\dot{\bar{\epsilon}}_0} \right) \\ \{E_{RT}\} &= \{E_0\} \left(1 + C_2 \ln \frac{\dot{\bar{\epsilon}}}{\dot{\bar{\epsilon}}_0} \right) \end{aligned} \quad (15)$$

Where

$$\begin{aligned} \{\dot{\bar{\epsilon}}\} &= \{|\dot{\epsilon}_1| \quad |\dot{\epsilon}_2| \quad |\dot{\epsilon}_1| \quad |\dot{\epsilon}_2| \quad |\dot{\epsilon}_{12}| \quad |\dot{\epsilon}_{13}| \quad |\dot{\epsilon}_{23}|\}^T \\ \{S_{RT}\} &= \{X_{1t} \quad X_{2t} \quad X_{1c} \quad X_{2c} \quad S_{12} \quad S_{13} \quad S_{23}\}^T \\ \{E_{RT}\} &= \{E_1 \quad E_2 \quad E_3 \quad G_{12} \quad G_{13} \quad G_{23}\}^T \end{aligned} \quad (16)$$

and the subscript RT refers to the rate-adjusted values, the subscript 0 refers to the static value, $\dot{\bar{\epsilon}} = 1^{-1}$ is the reference strain-rate, $\dot{\bar{\epsilon}}$ is the effective strain-rate, C_1 and C_2 are the strain-rate constants, respectively.

2.3 Cohesive elements and material properties

The resin layer at the interface between 0° lateral axis and oriented at 90° across its diameter plies was modelled using cohesive elements available in ABAQUS [ABAQUS Users Manual (2011)]. The elastic response was defined in terms of a traction-separation law with uncoupled behaviour between the normal and shear components. The default choice of the constitutive thickness for modelling the response, in terms of traction versus separation, is 1.0, regardless of the actual thickness of the cohesive layer. Thus, the diagonal terms in the elasticity matrix and density should be calculated using the true thickness of the cohesive layer as follows:

$$K_{nn} = \frac{E_n}{t_c}, \quad K_{ss} = \frac{E_s}{t_c}, \quad K_{tt} = \frac{E_t}{t_c}, \quad \rho = \rho_c t_c \quad (17)$$

The quadratic nominal stress and energy criterion were used to model damage initiation and damage evolution, respectively. Damage initiated when a quadratic interaction function, involving the nominal stress ratios, reached unity. Damage evolution was defined based on the energy conjunction with a linear softening law. The mechanical properties of the cohesive elements were obtained from [Karagiozova et al. (2010)].

3 Implementation of the material model in ABAQUS/Explicit

The user defined VUMAT subroutine was developed to implement the material model and failure criteria described in the previous sections in ABAQUS/Explicit. During each time step of computation, this subroutine is compiled and enables ABAQUS/ Explicit to obtain the required information regarding the state of the material and the material mechanical response at each integration point of each element. The Hashin's 3D failure criteria outlined in Eq. (7-10) are calculated, and the elastic modulus and strength values are adjusted for strain-rate effects using Eq. (14) base on these stresses computed within the VUMAT subroutine using the given strains and the material stiffness coefficients. The element status, which determined by the failure criteria, is then changed from 1 to 0 when an element fails. Accompanying the change of element status, the stresses at that material point are reduced to zero and it no longer contributes to the model stiffness. The element is removed from the mesh when all of the material status points of an element have been reduced to zero.

The 3D tube reinforced foam panel consisted of the foam, the composite and the cohesive layers as three separate parts. The PVC foam core and composite layers for CFRP tubes were meshed using C3D8R elements, which are eight-noded, linear hexahedral elements with reduced integration and hourglass control. The mesh generation and boundary conditions shown in Figure 2. The interfaces between the composite layers were created using eight-node 3D cohesive elements (COH3D8). The core size is 30×30×20 (in mm) and the diameters of the tube modelled included 8, 10 and 12.5 mm. The loading platens on both the top and bottom of the panel are meshed using rigid surface elements. The compressive load is applied to the top platen, with an only degree of freedom in the vertical direction. The bottom platen is fully fixed. Given that the panels were symmetric in nature, a half of each panel can be modeled with the appropriate boundary conditions applied along the planes of symmetry. A condition of general contact interaction was defined between the two neighboring layers of composites. Surface-based tie constraints were imposed between the composite layer and the cohesive layer to model adhesion between the adjacent layers. The contact interaction property for interaction between the foam and composite layer was also defined.

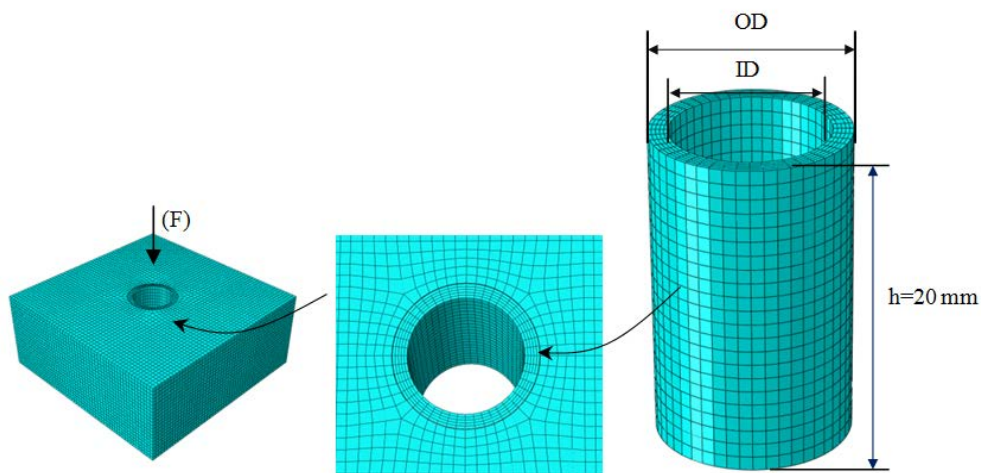


Figure 2 The geometry, mesh, boundary and loading conditions of the tube reinforced foam model.

4 Results and discussion

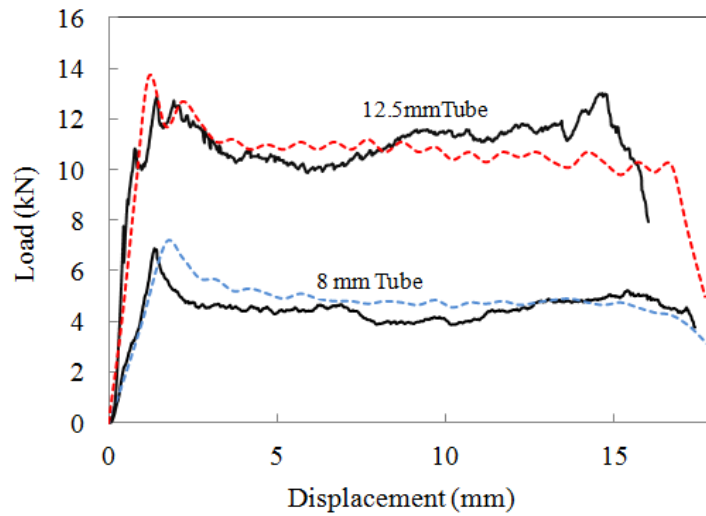


Figure 5 Load-displacement traces of individual carbon tube in diameter of 8, 10 and 12.5 mm under compression load.

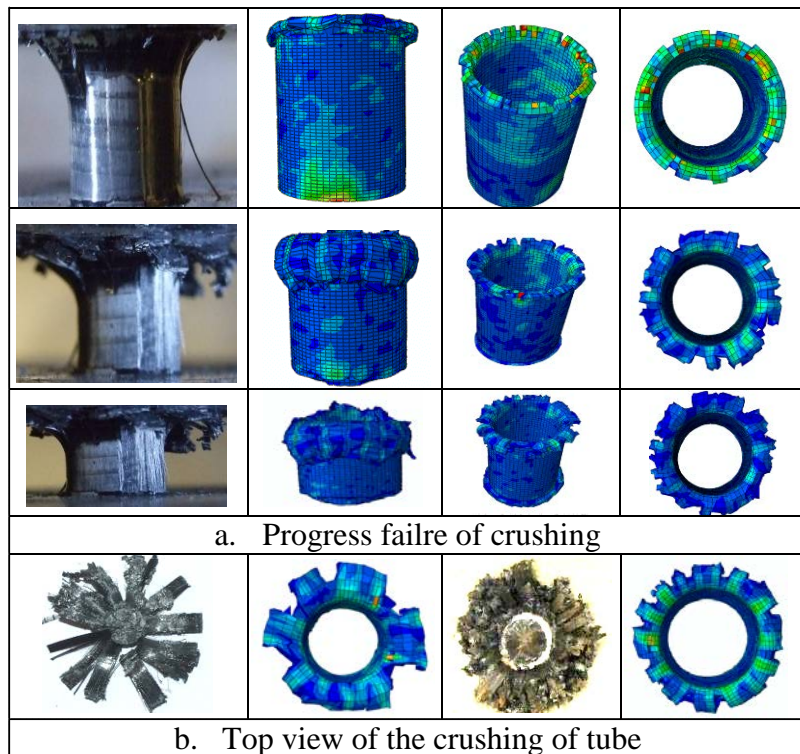


Figure 6 Comparison of progress deformation and failure for 10 mm CFRP tubes between test FE modeling.

The modeling for tube reinforced foam panel was developed based the rods reinforced foam. Prior to model the foam panel with embedded tube, the individual tube with foam support has been simulated and valuated with the experimental test on the tube. Figure 5 shows comparison of load-displacement traces obtained from FE prediction and the corresponding experimental results of the 8 and 12.5 mm tube individually. Reasonably good correlation has been obtained between the measurements and the numerical modeling in terms of the initial stiffness, the first peak load,

plateau load and damage evolution. It clearly shows that the predicted load from FE modelling is in a reducing trend after the first peak load during the compression process.

Figure 6 shows the comparison of progress deformation and failure for 10 mm CFRP tubes between test FE modelling. The basic features of the extensive splaying, fibre fracture and matrix cracking for the crushing tube were captured. The failed tubes is displayed the crushing states in which indicates a progress collapse of tubes. However, the failure modes of FE shows less extensive splaying of fibre may caused by the automatic remove of the failed element. The exact material data for the resin and fiber in longitudinal and circular direction can improve the failure modes.

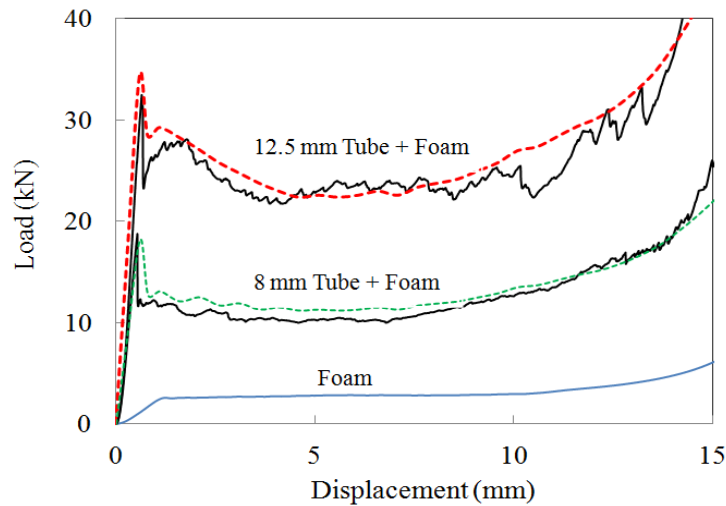


Figure 7 Comparison of load-displacement traces of C130 foam embedded in carbon tube in diameter of 8, 10 and 12.5 mm.

Here, PVC foam panels with densities of 40, 80 and 130 kg/m³ are embedded CFRP tubes in three diameters, i.e. 8, 10 and 12.5 mm. Figure 7 shows load-displacement traces obtained from numerical modeling and the corresponding experimental results of the 8 and 12.5 mm embedded in 130 kg/m³ PVC panel. The test results of a plain PVC foam panel without any CF tube are also shown in the figure to evident the enhancement of carbon tube. Again, agreements between the experimental results and the finite element simulations are very good, with well captured features in the initial stiffness, the peak load, the damage evolution and the densification. Clearly, the resistance load increased significantly up to a average plateau load of 11.3 and 22.7 kN for the 8, and 12.5 mm tube reinforced foam panel respectively. It noted that the plateau load of 12.5 mm reinforced form panel is 8 times of the plain form panel without embedded tube. It also indicates that the resistance force increased with diameter of embedded tube form 11.3 kN for the 8 mm tube to 22.7 kN for the 12.5 mm tube reinforced foam.

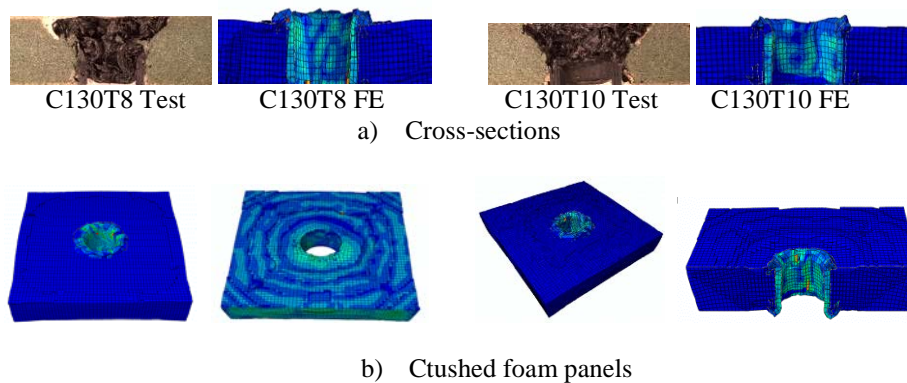


Figure 8 The comparison of cross-section on tube embedded foam and failure modes of crushed panel.

Figure 8 shows the cross-sections comparison of deformation and failure modes for C80 foam core panel with embedded CFRP tubes obtained from test and FE modelling. The core structure was deformed by 75% from its original configuration. The basic features of the foam crushing failure and the pin failure were captured. The failure modes of FE shows less crushing debris due to the failed elements removed automatic by the element control. The failed tubes is displayed the crushing states in which indicates a progress collapse of tubes embedded in the PVC foam. The more of the crushed failure modes of the tube reinforced panel are show in figures. The failure also indicates that strong constraint from the foam forces the CFRP tubes failure crushing along their longitudinal axis, which explains the enhancement of foam. However, the crushing failed elements in the modeling may cause element penetration with each other, which underestimates resistance of the tube to the compressive load.

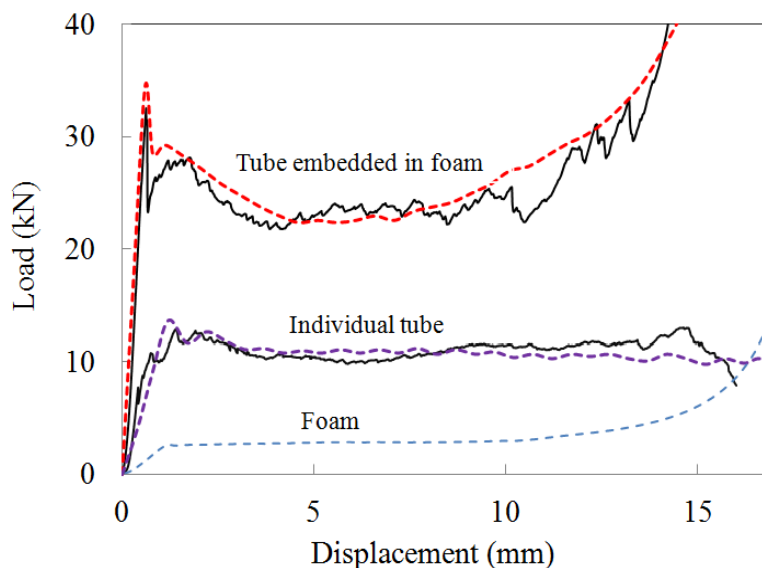


Figure 9 Comparison of load-displacement traces between individual carbon tube in diameter 12.5 mm and tube embedded in C130 foam under compression load.

The comparison of the load-displacement traces between individual tube, tube embedded in foam, and whole panel with a density of 130 kg/m^3 and embedded CF tube in diameters of 12.5 mm are exhibited in Figure 9. The dash line corresponding to the FE prediction whilst the solid line corresponding to the experimental test. An examination of the response of tube shows that the individual tube without foam constraint in a reduce trend during compression crushing, whilst the tube embedded in foam contribute huge resistance and energy absorption during crushing, also shows a increasing trend at the final stage of foam densification. The predicated load-displacement

cure of the embedded curve evident that the tube contribute over 80% load and energy absorption of foam panel and the embedded tube over perform more than twice of individual tube without foam support for the case of 12.5 mm tube embedded in C130 foam. This evidence clearly supports the suggestion that embedded tube in foam panel can modify the failure process and greatly enhance the crush performance of the tubes.

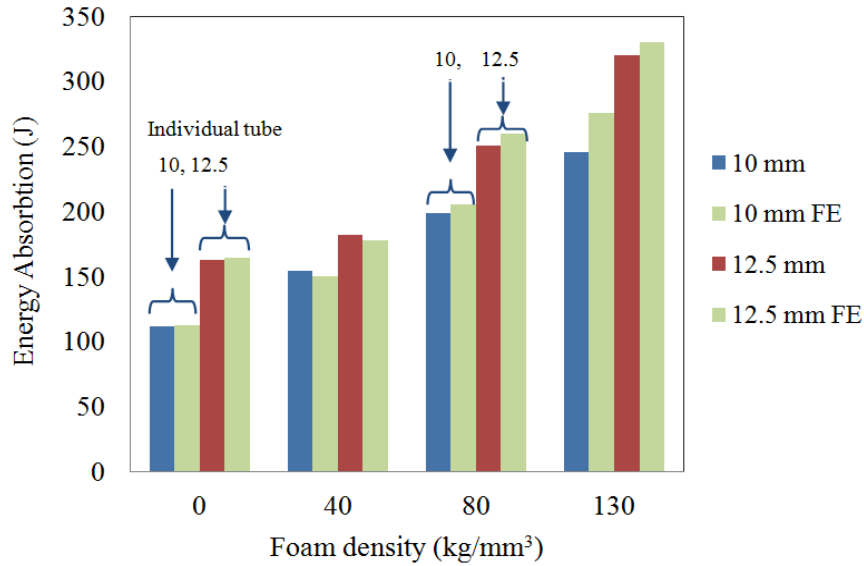


Figure 10 Comparison of energy absorption for individual tube and tube reinforced foam den between FE prediction and experimental test results.

Figure 10 shows the comprehensive comparison of energy absorptions obtained from experimental tests and FE predictions for individual and embedded carbon tube in diameters of 8, 10 and 12.5 mm in foam panel with density form 40 to 130 kg/mm³. The green bar is FE prediction in the bar chart. In general, correlation is quite good between test data and FE predication for the individual tube on the energy bar chart with a difference less than 5%, whereas the difference on the tube reinforced foam slight higher, which may caused by the estimated parameters for the interaction between tube and foam core. The FE predictions for the 40 kg/m³ foam panels are slightly lower than those of experimental measurements, whilst such the predictions for the higher density panels are slightly higher. The possible reason is that due to the weak constraint offered by the foam with the lower density foam, in the modeling such crushing causes element penetration with each other, which underestimates resistance of the tube to the compressive load. In the case of tube in higher density foam, the strong constraint from the foam forces the CFRP tubes failure crushing along their longitudinal axis, which offer continue resistance load without buckling failure and crushed totally. The FE simulation is ideal situation compare to the real state of experiment test.

Conclusions

User-defined constitutive models and strain-rate dependent failure criteria have been developed and implemented into finite element models to simulate load-displacement traces of PVC foam panels with embedded carbon fibre tubes, which are compared with the corresponding test results. Reasonably good correlation has been obtained between the experimental results and FE predictions, in terms of the initial stiffness, the peak load and the damage evolution. Here, three densities of the foam and three sizes of the CFRP tubes are investigated. In addition, energy absorption features of the sandwich core structures are captured by the modelling. The results show that the embedment of CFRP tubes inside PVC foam core is a very effective way to enhance energy absorption of this novel sandwich structure.

This evidence clearly supports the suggestion that embedded tube in foam panel can modify the failure process and greatly enhance the crushing performance of the tubes. This study also shows the advantage of FE modeling to predict and present the load of individual components for structural design analysis and optimization. The user-defined subroutines can be further developed to simulate more complex failure mechanisms of fibre reinforced composites.

References

- Alia R.A., Cantwell W.J., Langdon G.S., Yuen S.C.K., Nurick G.N., (2014), The energy-absorbing characteristics of composite tube-reinforced foam structures, *Composites: Part B*, 61, 127–135
- ABAQUS, *Theory Manual. Version 6.11* (2011). Pawtucket: Hibbitt, Karlsson & Sorensen, Inc.
- ABAQUS/Explicit, Users Manual, Version 6.11 (2011), Hibbitt, Karlsson & Sorensen, Inc.;
- Beard S.J., Chang F.K. (2002), Design of braided composites for energy absorption, *Journal of Thermoplastic Composite Materials*, 15, 3–12
- Cartie D. and Fleck N (2003), The effect of pin reinforcement upon the through-thickness compressive strength of foam-cored sandwich panels, *Composites Science and Technology*, Vol. 16, 2401-2409.
- Deshpande V.S.. and Fleck N.A. (2001) “Multi-axial yield behavior of polymer foams”, *Acta mater.*, Vol. 49, 1859–1866
- Farley, G. L. and Jones, J. M. (1986), Analogy for the effect of Material and geometrical variables on energy absorption capability of composite tube, *Journal of Composite Materials*, Vol. 20, 390-400
- Flesher, N.D. (2006), Crash Energy Absorption of Braided Composite Tubes *Ph. D. Thesis, Department of Mechanical Engineering, Stanford University, Stanford, CA, USA.*
- Farley, G. L. and Jones, J. M., Analogy for the effect of Material and geometrical variables on energy absorption capability of composite tube, *Journal of Composite Materials*, Vol. 20, 1986, pp. 390-400
- Guan Z.W, Aktas A., Potluri P., Cantwell W.J., Langdon G., Nurick G.N. (2014), The blast resistance of stitched sandwich panels, *International Journal of Impact Engineering* 65, 137e145
- Hashin Z. Failure criteria for unidirectional fiber composites(1980), *J Appl Mech.* 47,329–34.
- Hamada H. et al, (1993) 38th International SAMPE Symposium and Exhibition, 38, pp952-966.
- Jacob G. C., Fellers J. F. Simunovic, S., and Starbuck J. M. (2002), Energy absorption in polymer composites for automotive crashworthiness, *Journal of Composite Materials*, vol. 36, no. 7, 813–850,
- Karagiozova D, Langdon GS, Nurick GN, Yuen SCK (2010). Simulation of the response of fibre–metal laminates to localised blast loading. *Int J Impact Eng*;37(6):766–82.
- Mamalis, A.G, Manolakos, D.E, Ioannidis M.B, Papapostolou D.P. (2006), The static and dynamic axial collapse of CFRP square tubes: finite element modeling. *Composite Structures*, 74, 213–225
- McGregor C.J., Vaziri R., Poursartip A., Xiao X. (2007), Simulation of progressive damage development in braided composite tubes under axial compression. *Composites Part A: Applied Science and Manufacturing*, 38, 2247–2259
- Mc Gregor Carla, Vaziri Reza, Xiao Xinran, (2010) Finite element modelling of the progressive crushing of braided composite tubes under axial impact. *International Journal of Impact Engineering*, 37 662–672
- Mc Gregora Carla, Vaziri Reza, Xiao Xinran (2010), Finite element modelling of the progressive crushing of braided composite tubes under axial impact. *International Journal of Impact Engineering*, Volume 37, 6, 662–672
- Pinho S.T., Camanho P.P., Moura M.F. De, (2004), Numerical simulation of the crushing process of composite materials *International Journal of Crashworthiness*, 9, 263–276
- Rouse M., Ambur D.M., Bodine J. and Dopker B (1997). Evaluation of a composite sandwich fuselage side panel with damage and subjected to internal pressure. *NASA Technical Memorandum* 110309.
- Shockey A.A., Giovanola J.H., Simons J.W, Erlich D.C., Klopp R.W. and Skaggs S.R (1997). Advanced armor technology: application potential for engine fragment barriers for commercial aircraft, *Federal Aviation Administration Report* No. DOT/FAA/AR-97/53.
- Silcock M.D., Hall W. and Fox B.L. (2006), Finite element modeling of composite tubular crash structures with an explicit code, in 6th Annual SPE Automotive Composites Conference, 669–682.
- Thornton, P.H. (1979), Energy Absorption in Composite Structures, *Journal of Composite. Materials*, 13:247-262.
- Thornton, P. H. and Edwards P. J. (1982), Energy Absorption in Composite Tubes, *Journal of Composite Materials*, 16. 521–545.
- Vo TP, Guan ZW, Cantwell WJ, Schleyer GK,(2012). Low-impulse blast behaviour of fibre–metal laminates. *Composite Structures*, 94(3):954–65.
- Vo TP, Guan ZW, Cantwell WJ, Schleyer GK(2013). Modelling of the low-impulse blast behaviour of fibre–metal laminates based on different aluminium alloys, *Composites: Part B* 44, 141–151
- Xiao X., M. Botkin, Johnson N.L. (2009), Axial crush simulation of braided carbon tubes using Mat58 in LS-DYNA, *Thin-Walled Structures*, 47, 740–749
- Yen CF. Ballistic impact modeling of composite materials (2002). In: *Proceedings of the 7th international LS-DYNA users conference*, vol. 6. 15–23.
- Zhou J, Hassan M.Z., Guan Z.W. and Cantwell W.J (2012). The low velocity impact response of foam-based sandwich panels; *Composites Science and Technology*, 72, 1781-1790.